LEARNING NONLINEAR MANIFOLDS OF DYNAMIC TEXTURES

Ishan Awasthi
Department of Electrical and Computer Engineering, Rutgers University, Piscataway, NJ, USA

Ahmed Elgammal
Department of Computer Science, Rutgers University, Piscataway, NJ, USA

Keywords: Texture, Dynamic Texture, Image-based Rendering, Non Linear Manifold Learning.

Abstract: Dynamic textures are sequences of images of moving scenes that show stationarity properties in time. Eg: waves, flame, fountain, etc. Recent attempts at generating, potentially, infinitely long sequences model the dynamic texture as a Linear Dynamic System. This assumes a linear correlation in the input sequence. Most real world sequences however, exhibit nonlinear correlation between frames. In this paper, we propose a technique of generating dynamic textures using a low dimension model that preserves the non-linear correlation. We use nonlinear dimensionality reduction to create an embedding of the input sequence. Using this embedding, a nonlinear mapping is learnt from the embedded space into the image input space. Any input is represented by a linear combination of nonlinear bases functions centered along the manifold in the embedded space. A spline is used to move along the input manifold in this embedded space as a similar manifold is created for the output. The nonlinear mapping learnt on the input is used to map this new manifold into a sequence in the image space. Output sequences, thus created, contain images never present in the original sequence and are very realistic.

1 INTRODUCTION

Our aim is to design an algorithmic framework that allows the creation of photorealistic, yet, arbitrarily long sequences of images for a dynamic scene, based on a short input sequence of a similar scene. Variously referred to as Dynamic Textures (Soatto et al, 2001), Video Textures (Schödl et al., 2000) or Temporal Textures (Szummer et al., 1996), these are image sequences that model motion patterns of indeterminate spatial and temporal extent. Waves in water, grass in wind, smoke, flame, fire, waterfall, etc. are a few examples of phenomena that fall in this category.
There are two basic ways to approach this problem,
a) Physics based rendering
b) Image based rendering

Physics based rendering is primarily focused on creating a physical model derived from the standard principles, to recreate the dynamics of the system. To make the output a little more realistic, approximations are then introduced and the model is simulated to synthesize an output sequence. The main advantage of this technique is that it provides extensive manipulation capability and an avenue to use the model for scientific calculations. But this technique suffers from the disadvantage of being computationally expensive and being less photorealistic. Perry and Picard (Perry et al., 1994) and Stam et al. (Stam et al., 1995) depicted the power and use of physics based models to synthesize sequences of gaseous phenomena like fire, flame, smoke, etc. Hodgins et al. (Hodgins et al, 1998) proposed a physical model for synthesizing and studying walking gaits. These provided sequences which could be easily manipulated but failed to produce visually appealing outputs.

Image based rendering techniques are focused on the creation of visually appealing and realistic output sequences. These could either follow a procedural technique generating synthetic images by clever concatenation or repetition of image frames. Or, these could be based on a model of the visual signal of the input sequence. Schödl et al. (Schödl et al., 2000) used a procedural technique to carefully choose sub-loops of an original video sequence and

Awasthi I. and Elgammal A. (2006).
LEARNING NONLINEAR MANIFOLDS OF DYNAMIC TEXTURES.
In *Proceedings of the First International Conference on Computer Vision Theory and Applications*, pages 243-250
DOI: 10.5220/0001378202430250
Copyright © SciTePress

create new sequences. They found frames representing 'transition points', in the original sequence. By selecting the frames that did not end up at 'dead-ends', that is, places in the sequence from which there are no graceful exits, they created very realistic output sequences. But they only replayed already existing frames, and had to rely on morphing and blending to compensate for visual discontinuities. Sequences which did not have similar frames well spaced temporally, were very difficult to be synthesized. Many natural processes like fluids were thus, hard to synthesize. Kwatra et al. introduced a new seam finding and patch fitting technique for video sequences. They represented video sequences by 3D spatio-temporal textures. Two such 3D textures could be merged by calculating a 2D surface which could act as the optimal seam. However like in (Schödl et al., 2000), they first found transition points by comparing the frames of the input sequence. Then in a window of a few frames around this transition they found an optimal seam to join the two sequences, represented as 3D textures. Since they rely on transitions, they sometimes need very long input sequences to find similar frames and a good seam. Both (Schödl et al., 2000) and (13), offered little in terms of editability as the only parameter that could be controlled was the length of the output sequence. Simple control like slowing down or speeding up could not be achieved. It was only techniques based on a model of the visual signal in the input images, that provided this opportunity to control various aspects of the output. Szummer and Picard (Szummer et al., 1996) suggested a STAR model for generating temporal textures using an Auto Regressive Process (ARP). Fitzgibbon (Fitzgibbon et al., 2001) introduced a model based technique of creating video textures by projecting the images into a low-dimensional eigenspace, and modeling them using a moving average ARP. Here, some of the initial eigenvector responses (depicting non-periodic motions, like panning) had to be removed manually. Soatto et al. (Soatto et al, 2001) produced similar work. They modeled dynamic textures as a Linear Dynamic System (LDS) using either a set of principal components or a wavelet filter bank. They could model complex visual phenomena such as smoke and water waves with a relatively low dimensional representation. The use of a model not only allowed for greater editing power but the output sequences also included images that were never a part of the original sequence. However, the outputs were blurry compared to those from non-procedural techniques and for a few sequences the signal would decay rapidly and the intensity gets saturated. Yuan et al. (Yuan et al., 2004) extended this work by introducing feedback control and modeling the system as a closed loop LDS. The feedback loop corrected the problem of signal decay. But the output generated was still blurry. This is because these models assume a linear correlation between the various input frames.

In this paper, we propose a new modeling framework that captures the non-linear characteristics of the input. This provides clear output sequences comparable to those of the procedural techniques while providing better control on the output through model parameters. The organization of the paper is as follows: Section 2 describes the mathematical framework that forms the basis of our model. In section 3, we provide a brief overview of Non-Linear Dimensionality Reduction (NLDR). Section 4 describes the technique used to model the dynamics of the sequence in the embedded space. In section 5, we describe the methodology of transforming the model from the low dimension embedding space to the observed image space. Finally, section 6 presents the results of using our framework on a diverse set of input image sequences.

2 MODEL FRAMEWORK

In this section we summarize the mathematical framework that we use for modeling the dynamic texture. The existing image based techniques model the input visual signal ((Soatto et al, 2001),(Fitzgibbon et al., 2001),(Szummer et al., 1996)) for creating dynamic textures, using a linear dynamic system of the following form:

$$x_t = Ax_{t-1} + v_t,\ \ v_t \sim \mathbb{N}(0, \Sigma_v)$$
$$y_t = Cx_t + w_t,\ \ w_t \sim \mathbb{N}(0, \Sigma_w)$$

Here, $y_t \in R^n$ is the observation vector; $x_t \in R^r, r << n$ is the hidden state vector, A is the system matrix; C is the output matrix and v_t, w_t are Gaussian white noises driving the system. In such a system, the observation is a linear function of the state. The limitation of this system is that this captures only the linear correlation between subsequent images. The lack of non-linear characteristics, lead to an output sequence that is not as crisp and detailed as the input.

We, propose a new model based on non-linear dimensionality reduction, which overcomes this shortcoming. The state representation is nonlinearly related to the observation and therefore, the parameters learnt, effectively model the non-linearities relating to substructures and small movements in the input sequence. The framework we propose is:

$$x_t = Ax_{t-1} + v_t, \quad v_t \sim \mathbb{N}(0, \Sigma_v)$$
$$y_t = B\psi(x_t) + w_t, \quad w_t \sim \mathbb{N}(0, \Sigma_w)$$

Where, $y_t \in R^n$ is the observation vector; $x_t \in R^r, r << n$ is the hidden state vector, A is the system matrix; B represents the coefficients of non-linear mappings; $\psi(x)$ is a function incorporating the basis functions to be used with B to define the non-linear mapping and v_t, w_t are Gaussian white noises driving the system.

We use NLDR using Locally Linear Embedding (LLE)(Roweis et al., 2000) and isometric feature mapping (Isomap) (Tenenbaum et al., 2000), to achieve a nonlinear embedding of the sequence. Given such an embedding, we explicitly model the transitions using a spline curve. This models the nonlinear manifold of the texture. Using the embedding, a RBF nonlinear mapping is fitted to the observation which leads to the nonlinear observation model in section 5-equation (2).

3 NON-LINEAR EMBEDDING

The model based approaches use dimensionality reduction to extract compact representations of relevant characteristics defining the data variability. Two popular forms of dimensionality reduction are principal component analysis (PCA) and multidimensional scaling (MDS). Both PCA and MDS are eigenvector methods that model variations in high dimensional data. PCA, finds a low-dimensional embedding of the data points that best preserves their variance as measured in the high-dimensional input space by computing the linear projections in the directions of greatest variance using the top eigenvectors of the data covariance matrix. Metric MDS, computes the low dimensional embedding that best preserves pair-wise distances between data points. If these distances correspond to Euclidean distances, the results of metric MDS are similar to those of PCA. Both methods are simple to implement, and their optimizations do not involve local minima, making these a popular choice despite their inherent limitations as linear methods. However, most scenes of simple natural phenomena depict non-linear dynamics and linear dimensionality reduction fails to capture the factors defining these non-linear characteristics. To overcome this shortcoming, we use non-linear dimensionality reduction to project the images into a low dimensionality embedding space. This is achieved using either the LLE or the Isomap algorithm. The following sub-sections discuss these methods in brief.

3.1 Locally Linear Embedding (LLE)

According to the LLE framework (Roweis et al., 2000), given the assumption that each data point and its neighbors lie on a locally linear patch of the manifold (Roweis et al., 2000), each point (image frame) y_i can be reconstructed based on a linear mapping $\sum_j w_{ij} y_i$ that weights its neighbors contributions using the weights w_{ij}. In our case, the neighborhood of each point is determined by its K nearest neighbors based on the distance in the input space. The objective is to find such weights that minimize the global reconstruction error,

$$E(w) = \sum_i \; | y_i - \sum_i w_{ij} y_i |^2, \quad \text{where i, j} = 1 \cdots \text{N}$$

The weights are constrained such that w_{ij} is set to 0 if point y_j is not within the K nearest neighbors of point y_i. This will guarantee that each point is reconstructed
from its neighbors only. The weights obtained by minimizing the error in the above equation are invariant to rotations and re-scalings. To make them invariant to translation, the weights are also constrained to sum up to one across each row, i.e., the minimization is subject to $\sum_j w_{ij} = 1$. Such symmetric properties are essential to discover the intrinsic geometry of the manifold independent of any frame of reference. Optimal solution for such optimization problem can be found by solving a least-squares problem as was shown in (Roweis et al., 2000). Since the recovered weights W reflect the intrinsic geometric structure of the manifold, an

embedded manifold in a low dimensional space can be constructed using the same weights. This can be achieved by solving, for a set of points $X = \{x_i \in R^e, i = 1..N\}$ in a low dimension space, wherein, $e << d$, and that minimize: $E(x) = \sum |x_i - \sum w_{ij} x_i|^2$ where i, j = 1· · · N, and, the weights are fixed. Solving such problem can be achieved by solving an eigenvector problem as was shown in (Roweis et al., 2000).

3.2 Isomap Embedding

Isometric feature mapping (Tenenbaum et al., 2000), or Isomap, algorithm preserves the pair-wise distances between points in the image space. It adds the additional constraint of preserving the intrinsic geometry of the data as described by the geodesic manifold distances between all pairs of data points. For neighboring points, Euclidian distance provides a good approximation to geodesic distance. For faraway points, geodesic distance is approximated by adding up a sequence of "short hops" between neighboring points. These hops are computed by finding shortest paths in a graph with edges connecting neighboring data points. The algorithm as defined in (Tenenbaum et al., 2000) has three main steps:

The first step determines which points are neighbors on the manifold *M*, based on the distances $d_x(i, j)$ between pairs of points *i*, *j* in the high dimension, input space *X*. It either connects each point to all points within some fixed radius e, or to all of its K nearest neighbors. These neighborhood relations are represented as a weighted graph G over the data points, with edges of weight $d_x(i, j)$ between neighboring points. In its second step, Isomap estimates the geodesic distances $d_M(i, j)$ between all pairs of points on the manifold *M* by computing their shortest path distances $d_G(i, j)$ in the graph G. In the third and final step, MDS is applied to the matrix of graph distances $D_G = \{d_G(i, j)\}$, constructing an embedding of the data in a *d*-dimensional Euclidean space Y that best preserves this estimated intrinsic geometry. The coordinate vectors y_i for points in Y are chosen to minimize the cost function:

$$\mathrm{E} = \| \tau(\mathrm{D_G}) - \tau(D_Y) \|_{L^2}$$

Where, D_Y denotes the matrix of Euclidean distances $\{d_Y(i, j) = \| y_i - y_j \|\}$ and $\| A \|_{L^2}$ the L^2 matrix norm = $\sqrt{\sum_{i,j} A_{ij}^2}$. The τ operator converts distances to inner products, which uniquely characterize the geometry of the data in a form that supports efficient optimization. The global minimum of Eq. 1.2 is achieved by setting the coordinates y_i to the top d eigenvectors of the matrix $\tau(D_G)$.

4 LEARNING DYNAMICS

Non-Linear dimensionality reduction provides us a low dimensional embedding that closely captures the dynamics of the input sequence. Each input frame resides as a node on the embedded manifold. A new sequence, with similar dynamics, will also have a similar low dimensional embedding. The first step towards the creation of the output sequence is the creation of the output manifold in the same embedding space. To do so, first a model of the embedding is created and then this model is used to create a new manifold.

4.1 Modeling the Embedded Manifold

The non-linear dimensionality reduction techniques are used to create an embedding of the input sequence in 3D space. The embedded manifold is then modeled as a *3d-spline*. This is done by assuming consecutive frames to be equidistant in time and, using the 3D coordinates of each frame within the embedding space, to construct a piece-wise polynomial in each dimension. Thus, at any time t a point $A(x_t, y_t, z_t)$ on the embedding can be represented by

$$f(t) = (PPx(t), PPy(t), PPz(t))$$

Where, PPx, PPy and PPz are the piecewise polynomials fitting the *x, y and z* co-ordinates of the frames of the input sequence in the embedding space.

4.2 Creating the Output Manifold

The embedding manifold for the output is created by using the manifold for the input as a guide and walking through the embedding space. If T is the time used for an input sequence with m input frames, the average time-step between consecutive frames is

$$T_{av} = T / m$$

Starting at the first frame, and moving along the spline at steps equal to T_{av} would result in an exact trace of the input sequence. In order, to create a unique sequence, some noise is added to the time step between two consecutive frames. Also to allow for a rate of change of speed, an acceleration factor α is also introduced. Thus, the time step for the embedding for the output sequence can be represented as

$$T_{step} = \alpha T_{av} + \gamma$$

The use of T_{step} ensures the unique positioning of nodes representing frames of the output sequence, along the embedding manifold. However, the actual trajectory of the manifold for the output sequence still remains the same as that of the input sequence. In order to add variability to the trajectory for the output sequence, gaussian noise is also added to the 3d co-ordinates calculated by the piecewise polynomials PPx, PPy and PPz. The new spline function now becomes:

$$f_{new} = f(PPx(T_n) + \mu_x, PPy(T_n) + \mu_y, PPz(T_n) + \mu_z)$$

Where, μ_x, μ_y and μ_z represent Gaussian noise along x, y and z co-ordinates respectively. Thus, from a position at time T_{cur} on the output manifold, the next position is calculated as:

$$\begin{aligned} T_{cur} &= T_{cur} + T_{step} \\ Pos_{new} &= f_{new}(T_{cur}) \end{aligned} \qquad (1)$$

Using, (1) we are able to create a new manifold within the 3d-embedding space that is restricted to within a cylindrical, twisted, shell with the manifold of the input sequence forming the axis of this shell.

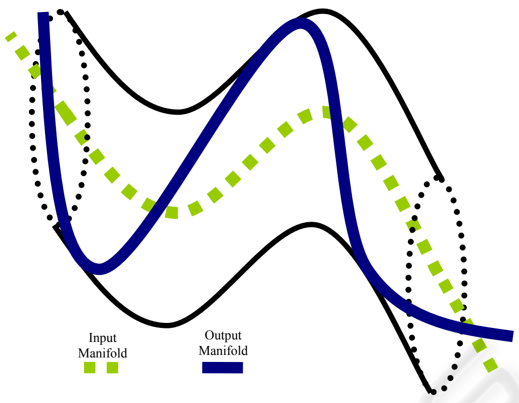

Figure 1.

5 OBSERVATION MODEL

Once the manifold in the embedding space has been modeled, we need to map points from the low dimensional embedding space into the high dimensional visual input space. In order to learn such nonlinear mapping, a Radial basis function interpolation framework is used. In the Radial basis functions interpolation framework, the manifold is represented in the embedding space implicitly by selecting a set of representative points along the manifold.

Let the set of representative input instances be $Y = \{y_i \in R^d \quad i = 1, \cdots, N\}$ and let their corresponding points in the embedding space be $X = \{x_i \in R^e, \quad i = 1, \cdots, N\}$ where e is the dimensionality of the embedding space (e.g. $e = 3$ in our case). We can solve for multiple interpolants $f^k : R^e \to R$, where k is k-th dimension (pixel) in the input space and f^k is a radial basis function interpolant, i.e., we learn nonlinear mappings from the embedding space to each individual pixel in the input space. The functions used are generally of the form:

$$f^k(x) = p^k(x) + \sum_{i}^{N} w_i^k \phi(|x - x_i|)$$

where $\phi(.)$ is a real valued basis function, w_i are real coefficients, $|.|$ is the norm on R^e (the embedding space) and p^k is a linear polynomial with coefficients c^k. The basis function we have used is the thin-plate spline $\phi(u) = u^2 \log(u)$. The whole mapping can be written in a matrix form as

$$f(x) = B.\psi(x) \qquad (2)$$

Where B is a $d \times (N+e+1)$ dimensional matrix with the k-th row $[w_1^k ... w_N^k \;\; c^{k^T}]$ and the vector $\psi(x)$ is $[\phi(|\mathrm{x} - \mathrm{x}_1|) \cdots \phi(|\mathrm{x} - \mathrm{x}_N|) \;\; 1 \;\; \mathrm{x}^T]^T$

The matrix B represents the coefficients for d different nonlinear mappings, each from a low-dimension embedding space into real numbers. To insure orthogonality and to make the problem well posed, the following additional constraints are imposed

$$\sum_{i=1}^{N} w_i p_j(x) = 0, \; j = 1, ..., m$$

where p_j are the linear basis of p. Therefore the solution for B can be obtained by directly solving the linear systems

$$\begin{pmatrix} A & P \\ P^T & 0 \end{pmatrix} B^T = \begin{pmatrix} Y \\ 0_{(e+1)\times d} \end{pmatrix}$$

Where, $A_{ij} = \phi(|x_j - x_i|), \quad i, j = 1...N$, P is a matrix with i-th row $[1 \;\; x_i^T]$ and Y is $(N \times d)$ matrix containing the input images $[y_1 ... y_N]^T$.

6 EXPERIMENTAL RESULTS

The algorithm was tested on various different input image sequences of varying length. The outputs were sequences with lengths, four times or greater than the input. Figure 2 shows the results for four sequences, each depicting different dynamics. The output sequences can be viewed online at http://www.cs.rutgers.edu/~elgammal/DynamicTexture. The input sequence for each was 70 frames in length. As can be seen, the synthesized images maintain both the dynamics and structure of the input. Depending on the shape of the input manifold, different approaches are used in generating the output manifold. The manifolds fell into one of three broad categories.

6.1 Closed Loop Embedding Manifold

When, the starting and the ending frames of the input sequence were either similar or at a small distance in the 3d-embedding space of the input manifold, the spline could be modified into a closed loop. This was achieved by introducing an edge between the first and the last points on the manifold (representing the first and the last frame) during the creation of the output manifold. The Flame, the Sparkling-ball and the Fountain sequences (Figure 2 (b),(c),(d)) show how the long output sequences, thus created. The output manifold for these sequences were created by looping around the closed loop of the input manifold as many times as was needed. Figure 3 (b), (c) & (d) show the manifold for the three sequences respectively.

6.2 Open Ended Embedding Manifold

When the starting and ending frames were far apart compared to the average distance between any 2 consecutive frames along the embedded manifold, closing the loop constituted a big jump and resulted in a jerk being introduced in the subsequently synthesized sequence. In such cases, the output manifold could be created by oscillating between the two extremes of the spline. However, this solution could be applied only to image sequences which already had some oscillation, like the beach and the turning face sequences. Figure 3 (a),(e) show the manifold for these, respectively.

6.3 Jerky Embedding Manifold

When, the input sequence comprises of relatively random and fast motion like in the boiling water sequence. The image frames are scattered within a small volume of the embedding space and the spline model constitutes a lot of sporadic jumps. In such a sequence, looping back to the first frame after the last has been reached, allows for a loop to be created with the associated jerk in the visual image space blending in with the rest of the jerks that the input sequence already depicts. Light and High-boiling water and the wavy river sequence have such a manifold. The manifold for the boiling water sequence is shown in Figure 3(f).

a)

b)

c)

d) 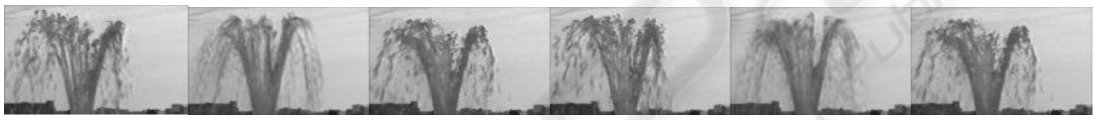

e) 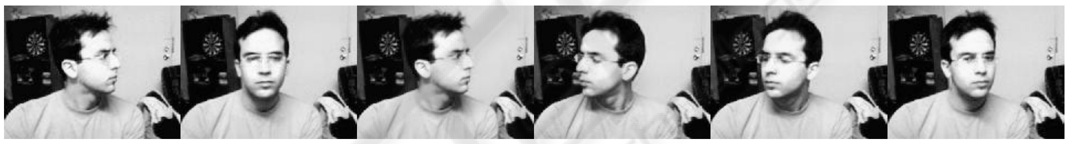

f) 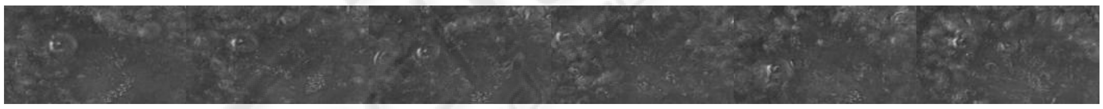

Figure 2: a)Beach, b)Flame, c)Sparkling Ball, d)Fountain, e)Face, f)Boiling Water.

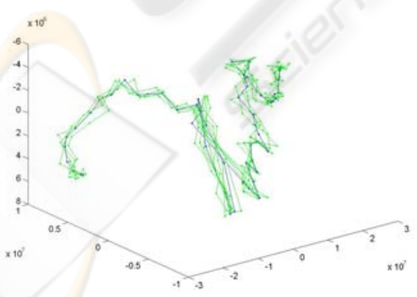

a)Beach

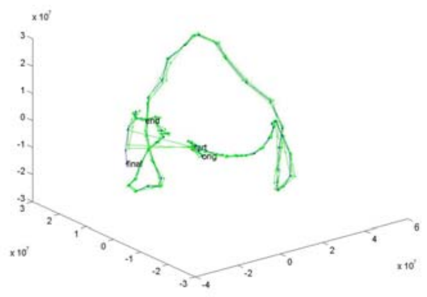

b)Flame

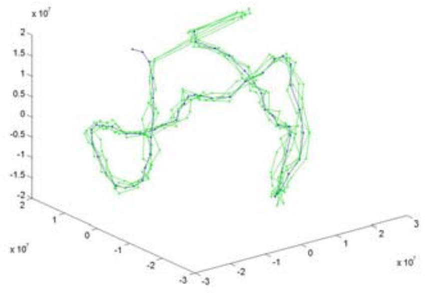
c)Sparkle

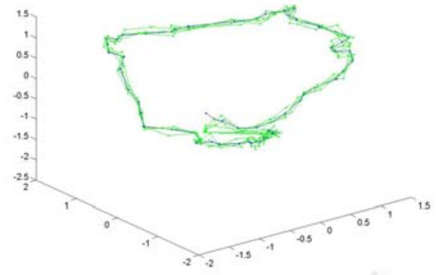
d)Fountain

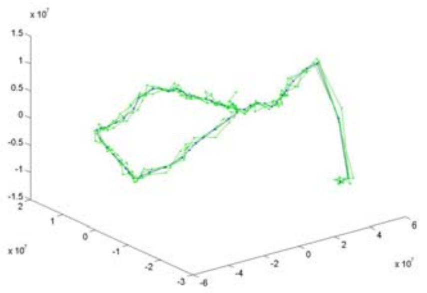
e)Face

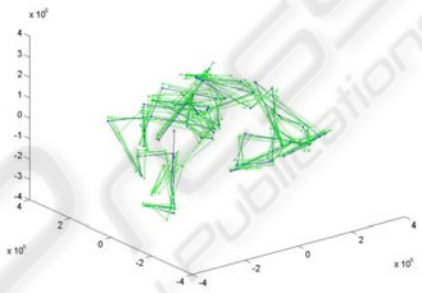
f)Boilingwater

Figure 3.

REFERENCES

J. Stam and E. Fiume. Depicting fire and other gaseous phenomena using diffusion processes. In Proc. SIGGRAPH '95, pages 129–136, August 1995.

J. K. Hodgins and W. L.Wooten. Animating human athletes. In Robotics Research: The Eighth International Symposium, pages 356–367, 1998.

J. Popovićć, S. M. Seitz, M. Erdmann, Z. Popovi´c, and A. Witkin. Interactive manipulation of rigid body simulations. In Proc. of SIGGRAPH '00, pages 209–218, July 2000.

C. H. Perry and R. W. Picard, "Synthesizing Flames and Their Spreading," Proc. of the 5th Eurographics Workshop on Animation and Simulation, Oslo, Norway, Sept. 1994.

A. Schödl, R. Szeliski, D.H. Salesin, I. Essa, Video textures, in: K.Akeley (Ed.), Siggraph 2000, Computer Graphics Proceedings, ACMPress/ACM SIGGRAPH/Addison Wesley/Longman, 2000, pp. 489–498.

A.W. Fitzgibbon, Stochastic rigidity: image registration for nowherestatic scenes, Proceedings of the Eighth International Conference On Computer Vision, 2001, pp. 662–669.

S. Soatto, G. Doretto, Y.N. Wu, Dynamic textures, International Conference on Computer Vision, 2001, pp. 439–446.

V. Kwatra, A. Sch¨odl, I. Essa, G. Turk and A. Bobick. Graphcut Textures: Image and Video Synthesis Using Graph Cuts. In Proceedings of Siggraph'03, pp. 277-286, 2003.

M. Szummer and R. W. Picard. Temporal Texture Modeling. IEEE International Conference on Image Processing, vol. 3, pp. 823-826, 1996.

L. Yuan, F. Wen, C. Liu, and H.Y. shum, "Synthesizing Dynamic Texture with Closed-Loop Linear Dynamical System", ECCV 2004, LCNS 3022, pp.603—616, 2004.

S. Roweis and L. Saul, Nonlinear dimensionality reduction by locally linear embedding, Science 290 (2000), 2323{2326.

J. B. Tenenbaum, V. de Silva, and J. C. Langford, A global geometric framework for nonlinear dimensionality reduction, Science 290 (2000), 2319{2323.